PAPER

Check for updates

Facile preparation of hybrid porous polyanilines for highly efficient Cr(VI) removal†

Wenjie Tang, Yue Wu, [ID]* Tingting Gao, Yingqin Wei [ID] and Guowei Zhou*

In the present work, leucoemeraldine-based hybrid porous polyanilines (LHPPs) have been synthesized by the Friedel–Crafts reaction of leucoemeraldine and octavinylsilsesquioxane (OVS) for Cr(VI) removal. The resulting LHPPs were characterized by Fourier transform infrared spectroscopy, powder X-ray diffraction, thermogravimetric analysis, scanning electron microscopy and N_2 adsorption–desorption. The findings indiated that the LHPPs were amorphous, with apparent surface areas (S_{BET}) in the range of 147 to 388 $m^2\ g^{-1}$ and total volumes in the range of 0.13 to 0.44 $cm^3\ g^{-1}$. Cr(VI) removal experiments displayed that the LHPPs exhibited highly efficient Cr(VI) removal performance. The maximum Cr(VI) removal capacity of **LHPP-1** was 990.1 mg g^{-1} at 308 K and pH 1, which is higher than those of other reported polyaniline-based adsorbents. The adsorption process was a spontaneous, endothermic and chemical adsorption process. The adsorption behavior agreed well with Langmuir models and pseudo second-order equations. X-ray photoelectron spectroscopy and Fourier transformed infrared (FTIR) spectroscopy analysis revealed that the highly efficient Cr(VI) removal performance can be mainly attributed to the existence of numerous amine and imine groups on the surface of the LHPPs; these can function as adsorption active sites for Cr(VI) removal through electrostatic adsorption and reduction to Cr(III) under acidic conditions. Moreover, the LHPPs exhibited excellent adsorption selectivity for Cr(VI) despite the presence of other metal ions (K^+, Cu^{2+}, Mn^{2+}) and anions (NO_3^-, SO_4^{2-}). Therefore, the LHPPs have potential applications for Cr(VI) removal in industrial wastewater.

1 Introduction

In the natural environment, chromium, a heavy metal ion, exists in two predominant forms.[1] Cr(III), one of the most commonly occurring forms of chromium in aqueous solutions, is less mobile, less soluble and less toxic. Moderate amounts of Cr(III) function as an essential micronutrient to organisms. However, excessive amounts of Cr(III) can give rise to allergic skin reactions.[2] In contrast, Cr(VI), the other common form of chromium in aquatic environments, is regarded as a major contamination source. It is extremely mobile and has mutagenic, teratogenic, carcinogenic and genotoxic effects on living organisms. With the rapid development of textile manufacturing, steel fabrication, leather tanning, paint fabrication, petroleum refining and electroplating, enormous quantities of chromium are being discharged into natural water systems, threatening the environment and human health.[3–5] The World Health Organization (WHO) recommends that the maximum concentrations of Cr(VI) ion for drinking water and industrial wastewater are 0.05 and

0.10 mg L^{-1}, respectively.[6,7] Therefore, in order to avoid damage from chromium, it is imperative to remove Cr(VI) and minimize the concentration of Cr(III) before chromium-contaminated water enters the ecosystem.

In the past decades, much work has been devoted to the wastewater treatment and environmental remediation of Cr(VI). The studied techniques include chemical precipitation, ion exchange, electrolysis, membrane filtration and adsorption.[8–10] Adsorption is the most promising approach due to its advantages of low cost, simple operation conditions, high efficiency and no secondary pollution. To date, on the basis of adsorption technology, numerous adsorbents have been developed to remove Cr(VI) from aqueous solution/wastewaters, including montmorillonite,[11] activated carbon,[12] metal and metal oxide,[13,14] metal–organic framework-based materials,[15] boron nitride-based materials,[16] double hydroxide-based nano-materials,[17] polymer-based nanocomposites,[18] and bio-adsorbents.[19] Although those adsorbents can effectively remove Cr(VI), most of them also have inherent disadvantages, such as lower removal capacities, high cost, and complicated and multiple steps for preparation and application.[1] Therefore, with the increasing requirements for economical removal of Cr(VI)-contaminated water, the development of novel adsorbents with the properties of high removal capacity, low cost, and ease of preparation and application is still a significant challenge.

Key Laboratory of Fine Chemicals in Universities of Shandong, School of Chemistry and Pharmaceutical Engineering, Qilu University of Technology (Shandong Academy of Sciences), Jinan 250353, Shandong, People's Republic of China. E-mail: yuewu_007@qlu.edu.cn; gwzhou@qlu.edu.cn; guoweizhou@hotmail.com

Recently, increasing attention has been given to polyaniline (PANI) because of its advantages of easy synthesis, low cost, stable chemical structure and perfect environmental compatibility.[20] As a common conducting polymer, PANI has been widely applied in the fields of catalysis, energy storage, anti-corrosion treatment and chemical and biological sensors.[21–24] Furthermore, using PANI as an adsorbent to remedy Cr(VI)-contaminated water has elicited great interest from researchers.[25] It is well-known that PANI has three oxidation states: leucoemeraldine, emeraldine and pernigraniline. PANI contains abundant amine and imine groups in these three states.[26] Under acidic conditions, Cr(VI) can be spontaneously reduced to Cr(III) by removing an electron from the –NH– unit. Meanwhile, the –N= unit can readily chelate the reduced Cr(III). Additionally, the amine and imine groups can be used as adsorption active sites to attract Cr(VI) through electrostatic attraction.[27] PANI is regarded as an effective and ideal adsorbent for removal of Cr(VI) through reduction and adsorption. However, bare PANI particles readily aggregate in the processes of application and preparation, resulting in slow kinetics and low adsorption capacity.[28,29] Moreover, pure PANI has poor porosity, which leads to low Cr(VI) removal capacity. Thus, in order to avoid the aggregation of PANI particles and greatly enhance the amounts of amine and imine groups on the adsorption material, many PANI composites, such as PANI@metal or metal oxides and PANI@carbon, have been prepared.[30] Although these PANI composites can effectively prevent the aggregation of particles and improve removal of Cr(VI), It is difficult to choose a proper substrate on which to load the adsorbent.[31,32] Additionally, to improve the porosity of PANI, templates, such as organic copolymers (polystyrene nanoparticle, block copolymer) and inorganic particles (SiO₂, zeolites and metal oxides), are commonly used due to their good structure controllability.[33–37] After polymerization, these templates are occasionally removed to obtain micro/nanoporous structures. Although those methods can significantly increase the porosity of polyaniline and provide relatively high removal capacities of Cr(VI), these studies often involve tedious operation processes. Furthermore, these processes cause enormous waste and sometimes introduce new heavy metal ions, resulting in secondary pollution.[38] Therefore, it is urgent to develop a facile and low-cost strategy to prepare porous polyanilines with large surface areas and high Cr(VI) removal capacities.[39]

Herein, we report a facile preparation of leucoemeraldine-based hybrid porous polyanilines (LHPPs) through a Friedel–Crafts alkylation reaction. In the reaction system, leucoemeraldine and OVS were used as the building block and cross-linker, respectively. Leucoemeraldine and OVS were connected by covalent bonds, which effectively prevents the aggregation of leucoemeraldine particles. The porous structure was directly obtained without removing the OVS. The preparation was facile and had no rigorous requirements or tedious steps. The obtained nanoporous LHPPs were amorphous polymers with apparent surface areas (S_{BET}) in the range of 147 to 388 m² g⁻¹. Then, the LHPPs were applied for highly efficient removal of Cr(VI); the synthetic route and the possible mechanism for Cr(VI) removal are shown in Scheme 1. To the best of our knowledge, this is the first time that the Friedel–Crafts alkylation reaction has been adopted to form porous polyanilines using leucoemeraldine and OVS as the building blocks. We investigated the removal performance of the LHPPs for Cr(VI) as well as the corresponding adsorption isotherms, adsorption kinetics, and adsorption thermodynamics. The results indicate that the nanoporous LHPPs contain abundant amine and imine groups which are mainly used as adsorption active sites for highly efficient adsorption and reduction of chromium(VI). The maximum removal capacity of **LHPP-1** for Cr(VI) is 990.1 mg g⁻¹ at 308 K, which is higher than those of other reported polyaniline-based adsorbents. This work provides a promising approach to remediate Cr(VI)-contaminated water which has highly promising application prospects.

2 Experimental

2.1 Materials and reagents

All chemical reagents used in the experiments were of analytical grade and were used directly without further purification unless otherwise specified. Aniline was purchased from Aladdin-Reagent Co. Ltd (Shanghai, China). 1,2-Dichloroethane (DCE), ammonium persulfate (APS), acetone, sulphuric acid, phosphoric acid, anhydrous aluminum chloride, potassium dichromate (K₂Cr₂O₇), sodium dithionite and 1,5-diphenylcarbazide were all purchased from Sinopharm Chemical Reagent Co. Ltd (Shanghai, China). DCE was purified by atmospheric distillation and stored with 4 Å molecular sieves. Octavinylsilsesquioxane (OVS) was prepared according to a previous literature report.[40]

2.2 Preparation of emeraldine

4.6 mL aniline and 50 mL hydrochloric acid solution (2 mol L⁻¹) were charged into a 250 mL round bottom flask in an ice-water bath. After stirring for 10 minutes, 25 mL ammonium persulfate (2 mol L⁻¹) was added dropwise to the reaction system. The aqueous solution became blackish green. After continuing the reaction for 4 h, the product was filtered and washed with deionized water, then transferred into 50 mL ammonia and stirred for 24 h. The product was filtered and washed with deionized water until the pH reached 7. Finally, the black powder was dried *in vacuo* at 60 °C for 12 h.

2.3 Preparation of leucoemeraldine

Emeraldine (4.0 g), sodium dithionite (8.0 g) and 40 mL deionized water were added to a 250 mL round-bottom flask. Under ambient temperature, after agitation for 6 h, another 4 g portion of sodium dithionite was added. While maintaining the reaction conditions, the mixture was continuously stirred for 12 h. Then, the powder was decanted into 500 mL of deionized water. After filtration, the brown powder was dried *in vacuo* at room temperature and stored in a desiccator under vacuum.
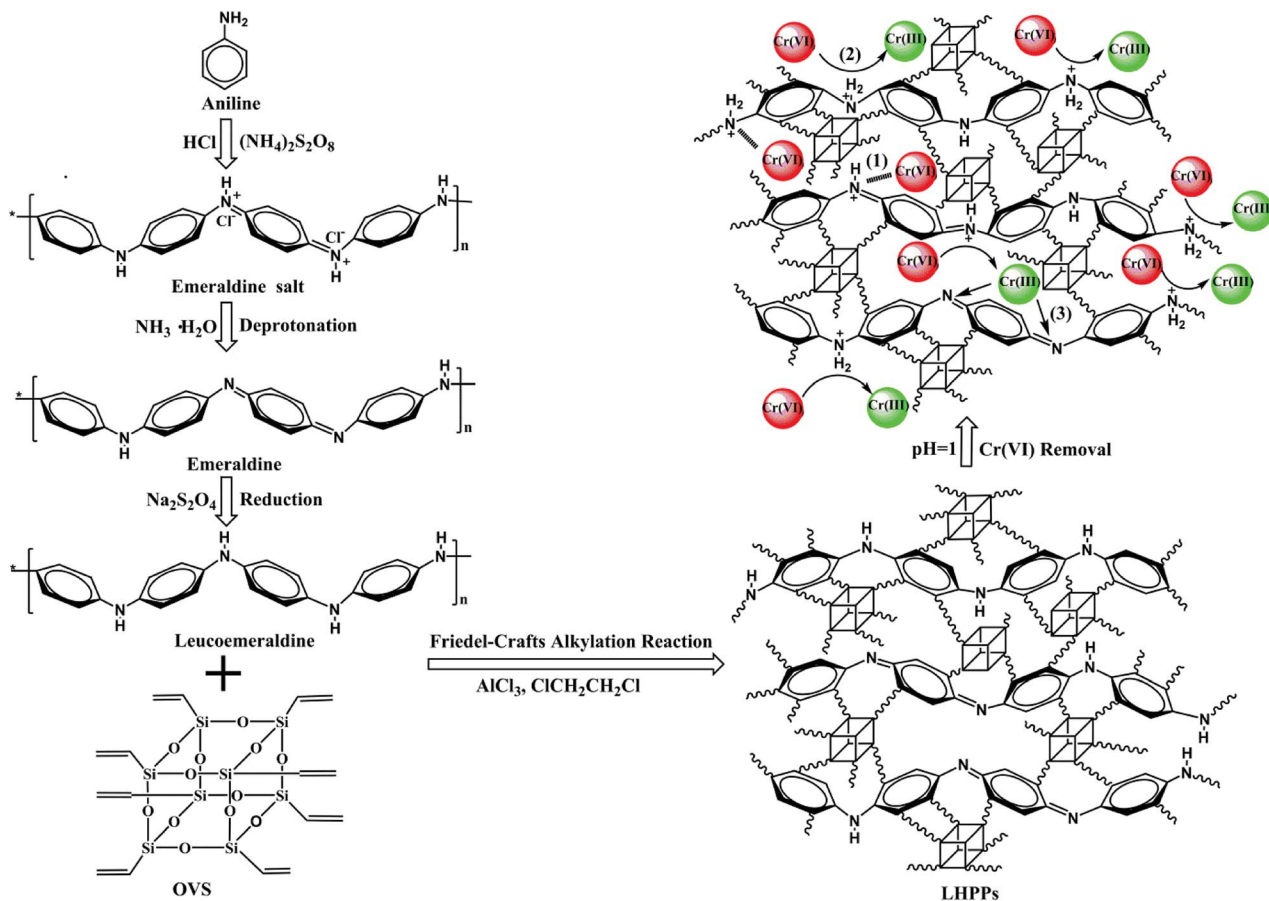
Scheme 1 Synthetic route for the LHPPs and proposed mechanism for Cr(VI) removal: (1) electrostatic attraction, (2) reduction, (3) chelation.

2.4 Synthesis of leucoemeraldine-based hybrid porous polyanilines (LHPP-1, LHPP-2 and LHPP-3)

1.0 g leucoemeraldine and a certain amount of OVS (0.3 g for **LHPP-1**; 0.5 g for **LHPP-2**; 0.7 g for **LHPP-3**) were poured into a 50 mL oven-dried one-necked flask. The reaction system was degassed and argon was input three times. Then, anhydrous AlCl$_3$ (2.00 g, 15 mmol) and 20 mL DCE were quickly loaded. The mixture was vigorously agitated at ambient temperature for 0.5 h and refluxed for 24 h. Then, the reaction system was cooled to room temperature. The product was washed with anhydrous methanol and collected by filtration. The powder was further washed with deionized water. Then, the obtained polymers were purified under a Soxhlet extractor with tetrahydrofuran and methanol for 48 h, respectively. Finally, the black powder was dried *in vacuo* at 60 °C for 12 h.

2.5 Adsorption experiment

A certain amount of K$_2$Cr$_2$O$_7$ was dissolved in deionized water to prepare a concentration gradient of Cr(VI) oxanion solutions (60 to 200 mg L^{-1}). Then, 30 mg as-synthesized porous polyaniline was dispersed in 200 mL of Cr(VI) solution. The mixture was shaken at 180 rpm with a thermostat oscillator. At a pre-set time, a 5 mL aliquot of the mixture was taken out and the supernatant was obtained by immediate centrifugation. The

equilibrium Cr(VI) concentration was determined using a UV-vis spectrophotometer with the diphenylcarbazide method, and the equilibrium adsorption capacity was calculated by the following equation:[41]

$$Q_e = \frac{(C_0 - C_e) \times V}{m} \tag{1}$$

where C_0 and C_e are the initial and equilibrium concentrations of the Cr(VI) solution, respectively; V is the volume of the Cr(VI) oxanion solution; and m is the mass of the adsorbent.

Each adsorption experiment was conducted thrice to evaluate the adsorption performance of the LHPPs. The effects of factors such as the level of acidity (pH 1 to 6), contact time (0 to 72 h), initial concentration of Cr(VI) oxanions (0 to 200 mg L^{-1}) and temperature (303 K, 308 K and 313 K) were investigated.

3 Results and discussion

3.1 Characterization of the LHPPs

Emeraldine was prepared according to a previous literature report.[42] The resulting emeraldine was deprotonated with ammonia and was then characterized by FT-IR spectroscopy (Fig. S1(b)†). The peaks at 3400, 1590, 1495, 1307 and 1160 cm^{-1} were ascribed to the N–H stretching vibration and C=N stretching modes of the quinonoid rings, the C=C stretching

vibration of the benzenoid rings, and the C–N stretching mode and N=Q=N quinonoid stretching vibration, respectively.[43] After reduction with aqueous sodium dithionite, the intensities of the peaks at 1590 and 1160 cm^{-1} in leucoemeraldine decreased to different degrees (Fig. S1(c)†). The results indicated that emeraldine was reduced to leucoemeraldine.[44] Emeraldine and leucoemeraldine were also characterized by UV-vis spectroscopy (Fig. S2†). The UV-vis spectra displayed that the peak of emeraldine at 640 nm disappeared after reduction with sodium dithionite; this phenomenon further confirmed that emeraldine had been transformed into leucoemeraldine. These results agreed with a previous report.[45]

Fig. S1(d–f)† displays the FT-IR spectra of **LHPP-1**, **LHPP-2** and **LHPP-3**, respectively. In comparison with the patterns of leucoemeraldine and OVS, the stretching vibration peaks of the C=C bending vibration in **LHPP-1** to **LHPP-3** were slightly red shifted; the value became about 1485 cm^{-1}. A new peak at about 2926 cm^{-1} appeared in the spectra of **LHPP-1**, **LHPP-2** and **LHPP-3**, and the intensities of the peaks increased to different levels. All these phenomena indicate that there were different contents of CH$_2$ groups in **LHPP-1** to **LHPP-3** after leucoemeraldine was reacted with OVS.[46,47] These results confirmed that leucoemeraldine participated in the Friedel–Crafts reaction.

Powder X-ray diffraction (XRD) was also used to analyze the crystallographic orders of emeraldine, leucoemeraldine, OVS, **LHPP-1**, **LHPP-2** and **LHPP-3**. As shown in Fig. 1, the sharp diffraction peaks at $2\theta = 15.1°$, 20.7° and 25.5° were ascribed to the (011), (020) and (200) crystal planes of emeraldine, confirming the existence of polyaniline in emeraldine form.[48] After reduction with aqueous sodium dithionite, no diffraction peaks emerged in the pattern of leucoemeraldine; this predictable result indicates that the leucoemeraldine was amorphous.[49] Additionally, the diffraction patterns of **LHPP-1**, **LHPP-2** and **LHPP-3** displayed that no distinct intensified diffraction peaks appeared, and only one broad peak appeared at approximately $2\theta = 23°$ in each polymer. These findings imply that the hybrid

nanoporous polyanilines of **LHPP-1**, **LHPP-2** and **LHPP-3** were amorphous and did not possess long-range ordered structures.[49]

The particle sizes and internal morphologies of the resulting nanoporous polymers were investigated by FE-SEM. As shown in Fig. 2(a), leucoemeraldine was composed of densely aggregated fibrous and granular particles.[50,51] After reaction with OVS, the hierarchical porous polymers were obtained (Fig. 2(b)–(d)).[52] The resulting hybrid polymers also comprised entangled irregular particles. The particle sizes of all these polymers were in the range of 100 nm to several tens of micrometers.

The thermal stabilities of leucoemeraldine, **LHPP-1**, **LHPP-2** and **LHPP-3** were investigated by TGA under N$_2$ atmosphere (Fig. S3†). The initial weight loss in the range of 40 °C to 120 °C was attributed to atmospheric water.[53] Compared with pure leucoemeraldine, from 120 °C to 300 °C, the weight losses of **LHPP-1**, **LHPP-2** and **LHPP-3** were related to removal of the HCl doping anions which were produced in the processes of preparation and purification.[53] From 300 °C to 1000 °C, the mass losses of leucoemeraldine and **LHPP-1**, **LHPP-2** and **LHPP-3** were ascribed to decomposition of the polymer chains.[53]

Fig. 3(a and b) displays the N$_2$ sorption isotherms and pore size distributions (PSDs) of **LHPP-1**, **LHPP-2** and **LHPP-3**. The three polymers exhibited steep N$_2$ uptakes at relatively low pressure ($P/P_0 < 0.001$), indicating the presence of abundant micropores in their structures.[49] At relatively high pressure, a slight hysteresis loop and a gradually increasing uptake were obtained. These results imply that these polymers possessed a certain number of mesopores and a few macropores.[49] It is also worth noting that the N$_2$ uptake isotherm of **LHPP-3** was slightly steeper than the other two isotherms at relatively high pressures, suggesting that the contributions of the mesopores and macropores in **LHPP-3** were greater than those in **LHPP-1** and **LHPP-2**. The PSD curves of **LHPP-1** and **LHPP-2** illustrate that the two hybrid polyanilines possessed uniform micropores centered at about 1.26 nm and a narrower distribution of mesopores from 2.1 nm to 10 nm; the PSD curve of **LHPP-3** exhibits that it possessed bimodal micropores centered at about 1.26 nm and a broader distribution of mesopores and macropores from 2.1 nm to 100 nm.
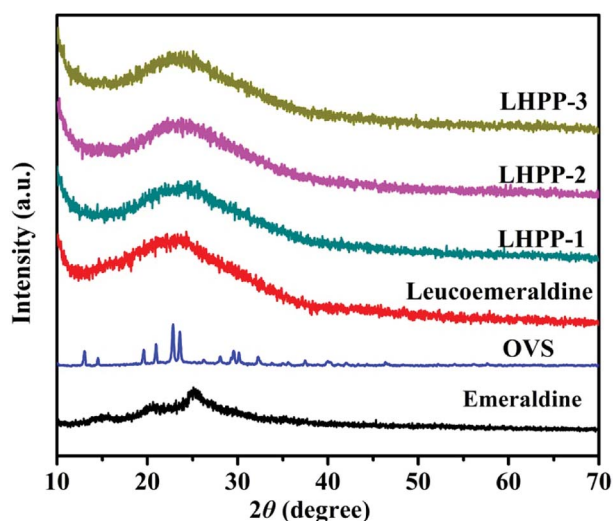

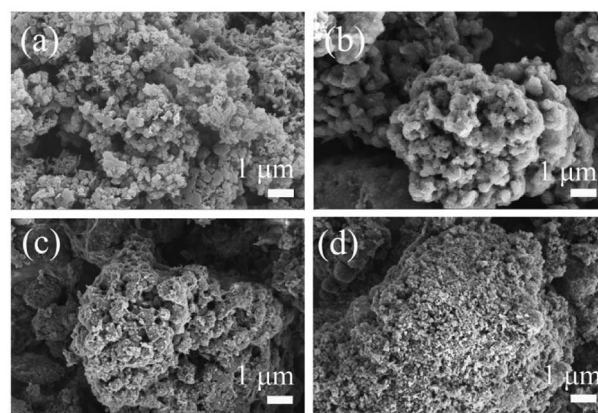Fig. 1 XRD patterns of emeraldine, leucoemeraldine, OVS, **LHPP-1**, **LHPP-2** and **LHPP-3**.

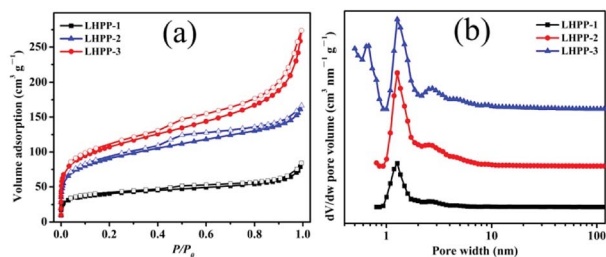Fig. 2 FE-SEM images of (a) leucoemeraldine; (b) **LHPP-1**; (c) **LHPP-2**; and (d) **LHPP-3**.

Fig. 3 (a) N$_2$ sorption isotherms of LHPP-1, LHPP-2 and LHPP-3; (b) pore size distributions of LHPP-1, LHPP-2 and LHPP-3.

The detailed porosity data of the three polymers are shown in Table 1. The apparent BET specific surface areas (S_{BET}) of **LHPP-1** to **LHPP-3** were 147, 330, and 388 m^2 g^{-1}, respectively. The total pore volumes (V_{total}) for **LHPP-1** to **LHPP-3** were 0.13, 0.26 and 0.42 cm^3 g^{-1} calculated at $P/P_0 = 0.99$, respectively. These high S_{BET} values and hierarchical pore structures can not only support more active adsorption sites but can also facilitate the transport of adsorbates in interconnected pore structure systems, thus enhancing the adsorption capacity.[38]

3.2 Cr(VI) removal performance of the LHPPs

3.2.1 Effects of pH. The acidity level has a significant effect on the adsorption capacity of Cr(VI). The solution pH can dramatically affect the existing forms of Cr(VI) and the surface charges of the polymer adsorbents, thereby affecting the removal capacity of the adsorbents. In view of the fact that **LHPP-1**, **LHPP-2** and **LHPP-3** possess similar chemical structures and physicochemical properties and that **LHPP-3** has the highest surface area, **LHPP-3** was firstly chosen as the sample to investigate the Cr(VI) removal capacity at different pH values. Adsorption experiments were performed with an initial Cr(VI) concentration of 200 mg L^{-1}, a contact time of 24 h, a temperature of 298 K, 30 mg of **LHPP-3**, and a pH range of 1 to 6 adjusted with 1 mol L^{-1} HCl and 0.1 mol L^{-1} NaOH aqueous solutions. As displayed in Fig. 4, the Cr(VI) removal capacity of **LHPP-3** was pH-responsive; that is, the adsorption capacity gradually increased with decreasing pH and reached its maximum of 558.7 mg g^{-1} at pH 1. These results can be attributed to two aspects. On the one hand, **LHPP-3** was constructed from OVS and leucoemeraldine. The resulting polymer was rich in –NH– and –N= groups in addition to its high surface area. At lower pH values, these groups are apt to be protonated and exist in the forms of –NH$_2^+$– and –NH$^+$=. Thus,

LHPP-3 possessed positive charges. Meanwhile, when the pH was in the range of 1 to 6, the primary existing forms of Cr(VI) ions were HCrO$_4^-$ and Cr$_2$O$_7^{2-}$. Thus, these positive charges produced strong electrostatic attractions with HCrO$_4^-$ and Cr$_2$O$_7^{2-}$, resulting in the successful removal of Cr(VI).[41] The contents of the protonated –NH$_2^+$– and –NH$^+$= groups increased with decreasing pH value. Consequently, the adsorption capacity of Cr(VI) increased with decreasing pH.[54] On the other hand, at relatively lower pH values, the main existing form of Cr(VI) is HCrO$_4^-$, which can be readily reduced to Cr(III) due to its higher redox potential.[55] In the subsequent experiments, the pH was adjusted to 1.

3.2.2 The effects of the component ratios. To study the effects of the composition of the LHPPs on their Cr(VI) removal performance and to obtain the optimum adsorption capacity, OVS, polyaniline, **LHPP-1**, **LHPP-2** and **LHPP-3** were used to conduct Cr(VI) adsorption experiments. The adsorption experiments were performed with adsorbent dosage: 30 mg, initial concentration: 200 mg L^{-1}, temperature: 298 K, contact time: 72 h, and shaking rate: 180 rpm. The equilibrium removal capacities of OVS and polyaniline were 0 and 10.35 mg g^{-1}, respectively. As shown in Fig. 5, the equilibrium removal capacities of **LHPP-1**, **LHPP-2** and **LHPP-3** were 963.7, 707.6 and 670.4 mg g^{-1}, respectively. The removal capacity for Cr(VI) decreased with increasing mass ratio of OVS and leucoemeraldine. These findings can be explained as follows: (i) in one aspect, as the mass ratios of OVS and leucoemeraldine increased, the S_{BET} of the LHPPs increased, which resulted in increased removal capacity for Cr(VI); (ii) in another aspect, with increasing mass ratio of OVS and leucoemeraldine, the content of leucoemeraldine units in the polymer structure decreased, resulting in lower contents of –NH– and –N= groups in the polyaniline structure.[27] Therefore, the amount of adsorption active sites decreased, leading to decreased removal capacity of Cr(VI). However, the decreases in the removal capacities originating from the gradually lower contents of –NH– and –N= groups were larger than the increases in the removal capacities arising from the gradually increasing S_{BET}; thus, finally, the removal capacities for Cr(VI) gradually decreased with increasing mass ratio of OVS and leucoemeraldine. In the subsequent experiments, **LHPP-1** was selected as the sample.

3.2.3 Effects of contact time and adsorption kinetics study. The effects of contact time on the removal capacity were also investigated. The adsorption experiments were performed with an oscillating rate of 180 rpm, a temperature of 308 K, 30 mg **LHPP-1** and an initial Cr(VI) concentration of 200 mg L^{-1}. The

Table 1 The porosity data for LHPP-1 to LHPP-3

Sample	OVS/leucoemeraldine (g g^{-1})	$S_{BET}{}^a$/m^2 g^{-1}	$S_{micro}{}^b$/m^2 g^{-1}	$V_{total}{}^c$/cm^3 g^{-1}	$V_{micro}{}^d$/cm^3 g^{-1}	V_{micro}/V_{total}
LHPP-1	0.3/1.0	147	123	0.13	0.05	0.38
LHPP-2	0.5/1.0	330	267	0.26	0.14	0.54
LHPP-3	0.7/1.0	388	220	0.42	0.10	0.24

^{a} Surface areas calculated from N$_2$ adsorption isotherms using the BET method. ^{b} Microporous surface areas calculated from N$_2$ adsorption isotherms using the t-plot method. ^{c} Total pore volumes calculated at $P/P_0 = 0.99$. ^{d} Micropore volumes derived using the t-plot method based on the Halsey thickness equation.
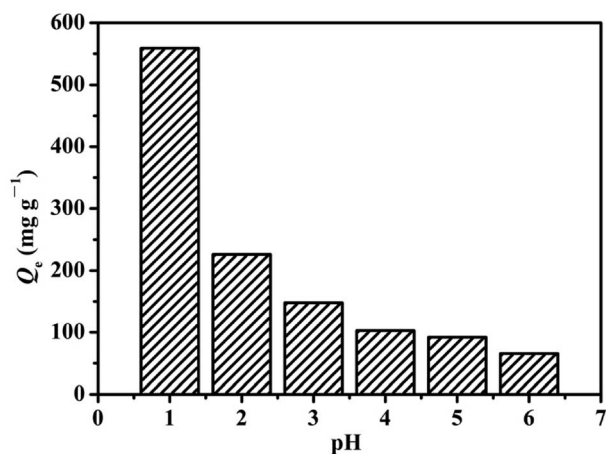
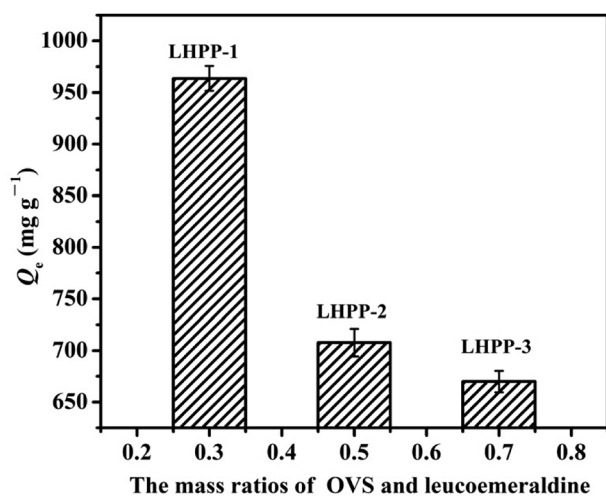Fig. 4 Effects of initial pH on the Cr(VI) removal performance of LHPP-3.

Fig. 5 Effects of the mass ratio of OVS and leucoemeraldine on the Cr(VI) removal performance of the samples.

relationship between the removal capacity at time t (Q_t) and the contact time is shown in Fig. 6(a). In the initial 5 h, **LHPP-1** exhibited a steep adsorption for Cr(VI), and the removal capacity was about 626.5 mg g^{-1}. Subsequently, the removal capacity

increased slowly until the maximum removal capacity of approximately 990 mg g^{-1} was obtained at about 48 h, indicating that the adsorption equilibrium was reached. This phenomenon is due to the continuously decreasing adsorption sites and the high concentration of Cr(VI) ions as well as the gradually increasing repulsive interactions.[56] In the initial stage of adsorption, at a lower pH and a high concentration of Cr(VI), many Cr(VI) ions could be quickly removed by **LHPP-1** in a short time because **LHPP-1** possesses sufficient adsorption active sites and a high surface area. As a large number of adsorption sites became occupied by Cr(VI) and Cr(III) ions, the number of adsorption sites and the concentration of Cr(VI) ions both decreased. In addition, the repulsive interactions between the Cr(VI) ions in solution and the negative charges in the solid phase significantly increased.[56] Therefore, after several hours of adsorption, it was difficult for the fewer remaining adsorption sites to uptake Cr(VI) ions from solution, resulting in a long time to reach equilibrium.

To better understand the adsorption behavior of **LHPP-1**, its Cr(VI) adsorption kinetics were further evaluated by the pseudo-first-order kinetic model and pseudo-second-order kinetic model, which assume that one Cr(VI) can occupy one or two adsorption sites on the surface of the adsorbent, respectively.[57]

Pseudo-first-order:

$$\log(Q_e - Q_t) = \log Q_e - \frac{K_1 t}{2.303} \tag{2}$$

Pseudo-second-order:

$$\frac{t}{Q_t} = \frac{1}{K_2 Q_e^2} + \frac{1}{Q_e} \tag{3}$$

where Q_t is the adsorption capacity of **LHPP-1** at time t (h) and K_1 and K_2 are the pseudo-first-order and pseudo-second-order adsorption rate constants, respectively.

Fig. 6(b and c) depicts the adsorption kinetics plots where the data were fitted by the pseudo-first-order and pseudo-second-order models. The detailed data are listed in Table 2. Obviously, the correlation coefficient ($R^2 = 0.995$) fitted with the pseudo second-order model was higher that fitted with the pseudo first-order model ($R^2 = 0.646$), indicating that Cr(VI) adsorption in this experiment was governed by chemical
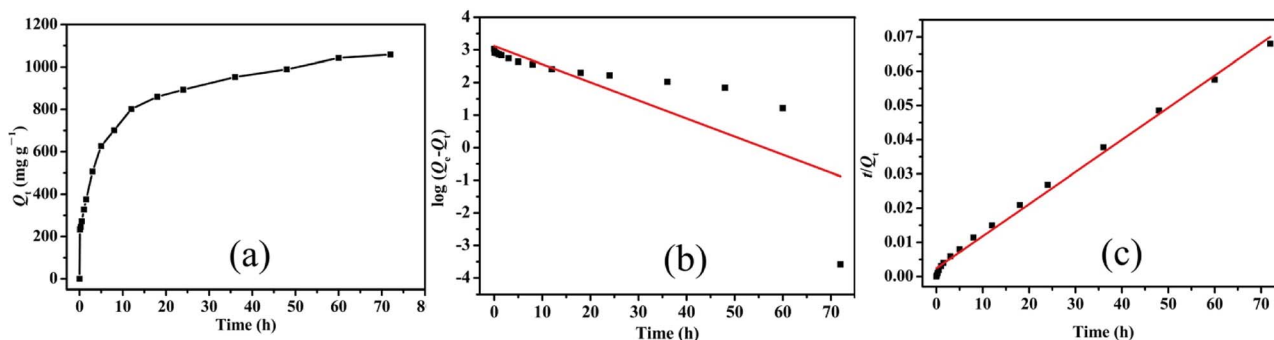

Fig. 6 (a) Relationship of Q_t and contact time with Cr(VI) removal by **LHPP-1** and adsorption kinetics studies with the (b) pseudo-first order model and (c) pseudo-second order model.

Table 2 The detailed data of the adsorption kinetic equations

	Pseudo-first-order			Pseudo-second-order		
Adsorbate	K_1	Q_e	R^2	K_2	Q_e	R^2
Cr(VI)	0.128	1304.2	0.646	0.000366	1064.9	0.995

adsorption and that one Cr(VI) could occupy two adsorption sites.[57]

3.2.4 Effects of initial concentration and adsorption isotherm study. To explore the effects of the initial concentration of Cr(VI) on the removal performance of **LHPP-1**, adsorption experiments were carried out with a temperature of 308 K, 30 mg of **LHPP-1**, and initial Cr(VI) concentrations in the range of 60 to 200 mg g^{-1}. The results are shown in Fig. 7(a). At lower initial concentrations, the equilibrium adsorption capacity (Q_e) increased with increasing initial concentration of Cr(VI). This is probably because higher concentrations of Cr(VI) can shorten the mean free path and increase the collisions between Cr(VI) and the adsorption sites of **LHPP-1**, thereby promoting the transportation of Cr(VI) ions from the solution to the adsorbents. With continuously increasing initial concentration of Cr(VI), the adsorption sites supported by **LHPP-1** could not satisfy the requirements to remove Cr(VI) from the solution; then, Q_e reached its maximum value of 1003 mg g^{-1}. Subsequently, Q_e did not change further despite the increase of the initial concentration of Cr(VI). This phenomenon is due to the high S_{BET} and the electrostatic attraction between the adsorbent–adsorbate system.[41]

The Langmuir and Freundlich isothermal models were both used to simulate the adsorption process. The Langmuir model assumes that there are no interactions between the adsorbed molecules and that monolayer adsorption occurs (chemisorption). The Freundlich model is an empirical model on the basis of sorption on heterogeneous surfaces, assuming that the stronger binding sites are basically occupied and the binding strength decreases with increasing degree of site occupation. The adsorption isotherm data were calculated by the Langmuir and Freundlich isotherm models, respectively. The linear forms were shown by the following equations:[58]

Langmuir isotherm model:

$$\frac{C_e}{Q_e} = \frac{1}{K_L Q_m} + \frac{C_e}{Q_m} \tag{4}$$

Freundlich isotherm model:

$$\log Q_e = \log K_F + \frac{1}{n} \log C_e \tag{5}$$

The dimensionless quantity of the Langmuir isotherm model, termed the separation factor (R_L), was calculated by the following equation:

$$R_L = \frac{1}{1 + K_L C_0} \tag{6}$$

where C_e (mg L^{-1}) and C_0 (mg L^{-1}) represent the equilibrium concentration and initial concentration; Q_e (mg g^{-1}) and Q_m (mg g^{-1}) denote the adsorption capacity at equilibrium and the maximum adsorption capacity in the calculation, respectively; K_L and K_F are the adsorption constants of the Langmuir and Freundlich adsorption isotherm models, respectively; and n is the adsorption intensity.

Fig. 7(b) and (c) depicts the adsorption equilibrium data fitted by Langmuir and Freundlich isotherm models. The detailed data calculated by the two isotherm models are listed in Table 3. The correlation coefficient (R^2) calculated by the Langmuir isotherm model was 0.999, which is higher than that of the Freundlich model ($R^2 = 0.404$). This result indicates that the Cr(VI) ion removal process in this work conformed well with the Langmuir isotherm model and that the adsorption process was monolayer chemisorption.[3] Moreover, the value of R_L was 0.898 and fell in the range of 0 to 1, suggesting the favorable uptake of Cr(VI).[58] The calculated Q_m was 990.1 mg g^{-1}, which is close to the experimental data. The maximum removal capacity of **LHPP-1** is higher than those of other reported polyaniline-based adsorbents and other adsorbents, as shown in Table 4.

3.2.5 Effects of temperature and adsorption thermodynamic study. Thermodynamic studies of Cr(VI) removal by **LHPP-1** were performed at 303, 308 and 313 K to investigate the nature of the removal process. Fig. 8(a) shows the relationship between the equilibrium adsorption quantity and the solution
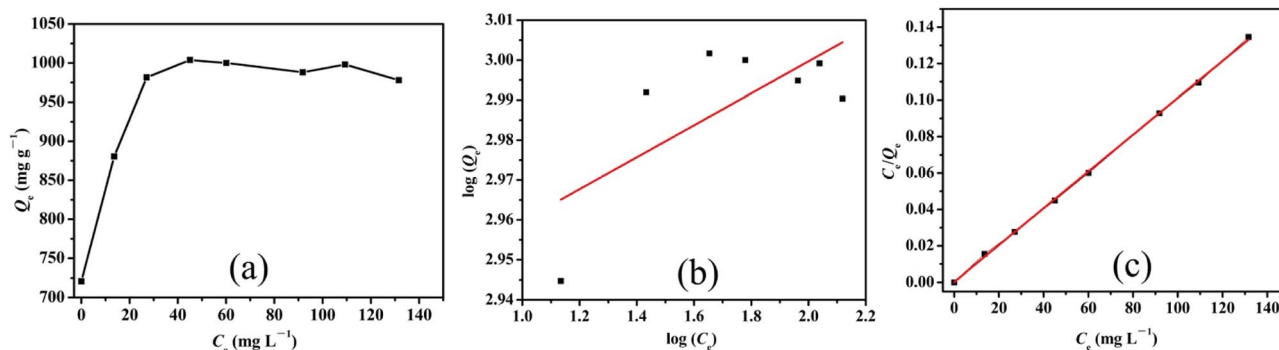

Fig. 7 (a) Effects of the initial concentration on Cr(VI) removal by **LHPP-1** and adsorption isotherm studies with the (b) Freundlich isotherm model and (c) Langmuir isotherm model.

Table 3 The detailed data of the adsorption isotherm models

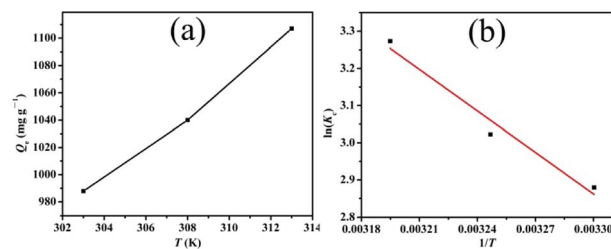| Adsorbate	Langmuir isotherm model				Freundlich isotherm model		
	K_L	Q_m	R_L	R^2	K_F	$1/n$	R^2
Cr(VI)	0.0005	990.1	0.898	0.999	831	0.04	0.404

Fig. 8 (a) The relationship of equilibrium adsorption capacity and solution temperature and (b) the van't Hoff equation model for the adsorption of Cr(VI) by LHPP-1.

temperature. With increasing temperature, the equilibrium adsorption capacity gradually increased. This is mainly attributed to Brownian motion; that is, with increasing temperature, the molecular motion became more vigorous, resulting in greatly increased collision probability between the adsorption active site and Cr(VI). The adsorption thermodynamic parameters were calculated by the following equations:[60]

$$\Delta G^0 = -RT \ln K_c \tag{7}$$

$$\ln K_c = \frac{\Delta S^0}{R} - \frac{\Delta H^0}{RT} \tag{8}$$

where ΔG^0, ΔS^0 and ΔH^0 are the standard Gibbs free energy change, standard entropy change and standard enthalpy change, respectively. K_c refers to the ratio of the Cr(VI) equilibrium adsorption quantity and equilibrium concentration. R is the gas constant (8.314 J mol^{-1} K^{-1}). T (K) is the absolute temperature.

Fig. 8(b) displays the relationship between $\ln K_c$ and $1/T$ calculated by the van't Hoff equation (eqn (8)). Through linear fitting, the slopes and intercepts were obtained. With the aid of these data, the values of ΔH^0 and ΔS^0 were calculated (Table 5). Obviously, the value of ΔH^0 is positive, indicating that the nature of the adsorption process is endothermic. Additionally, the positive value of ΔS^0 indicates that the affinity of LHPP-1 and Cr(VI) increased the randomness at the solid-solution interface. Moreover, the negative values of ΔG^0 exhibit that the adsorption process is spontaneous, implying that high temperature is beneficial for the adsorption process.

3.2.6 Effects of coexisting ions. In industrial waste water, Cr(VI) anion inevitably coexists with other metal cations or anions, such as K$^+$, Cu^{2+}, Mn^{2+}, NO$_3^-$ and SO$_4^{2-}$. These ions compete slightly with Cr(VI) ions and affect the Cr(VI) adsorption.[68] Therefore, it is worth studying the competitive adsorption effects of these coexisting ions on the removal performance of the adsorbent. The competitive adsorption experiments were performed under the conditions of pH 1, a temperature of 308 K, an oscillating rate of 180 r, an adsorbent dosage of 30 mg, an initial Cr(VI) concentration of 200 mg L^{-1}, and a contact time of 72 h. The molar ratio of the Cr(VI) anion and the coexisting ions was set at 1 : 1. The results are displayed in Fig. 9. In the absence of coexisting ions in the mixture, the equilibrium adsorption capacity of Cr(VI) anion was 1040.55 mg g^{-1}. Meanwhile, in the presence of K$^+$, Cu^{2+} and Mn^{2+} ions, the equilibrium adsorption amounts of Cr(VI) slightly decreased to 1014.95, 965.57 and 925.66 mg g^{-1}, respectively. These findings suggest that the metal ion species present in the reaction solution competed for binding onto the sorption sites of the LHPP-1 surface. The probable reason is that in the presence of the coexisting cations, the nitrogen-containing groups in LHPP-1 inevitably chelated with the cations possessing empty orbits, such as Cu^{2+} and Mn^{2+}, resulting in a decrease in the number of adsorption active sites for Cr(VI) anion.[28] In the presence of both NO$_3^-$ and SO$_4^{2-}$ anions, the equilibrium adsorption amounts Cr(VI) slightly decreased to 1020.61 and 926.66 mg g^{-1}. SO$_4^{2-}$ affected the Cr(VI) removal capacity more significantly than NO$_3^-$; this may be due to the consumption of SO$_4^{2-}$ ions by the surface sites of LHPP-1 and, hence, a decrease of the available adsorption sites for Cr(VI) ions. Furthermore, SO$_4^{2-}$ ions decrease the surface positive charge and thereby decrease the electrostatic interactions between the surface and the Cr(VI) species.[68] Generally, regardless of the presence of these coexisting cations and anions, the equilibrium adsorption amounts for Cr(VI) were all greater than 920 mg g^{-1}; these results indicate that the affinity between Cr(VI) and LHPP-1 is very strong and

Table 4 Comparison of maximum adsorption capacities for Cr(VI) with other reported work

Adsorbent	Maximum adsorption capacity (mg g^{-1})	Ref.
pTSA-Pani@GO-CNT	142.85	59
PNEANI/Ch-HCl	229.8	7
PANI/HA	173.0	8
ZVI@C@PANI	508	55
Polyaniline@Ni(OH)$_2$	625	60
EPS@PANI	913.2	38
PANI/H-TNB	156.94	61
PVP/MoS$_2$	142.24	62
CHFs	112.71	63
LDHs@MoS$_2$	76.3	64
MPC-300	21.23	65
nZVI/MCM	164.31	66
C@La–TiO$_2$	50.5	67
LHPP-1	990.1	This work

Table 5 Thermodynamic parameters for Cr(VI) removal

Adsorbent	ΔH^0 (kJ mol^{-1})	ΔS^0 (J mol^{-1} K^{-1})	ΔG^0 (kJ mol^{-1})	T (K)
LHPP-1	30.98	126.02	−7.25	303
			−7.74	308
			−8.52	313
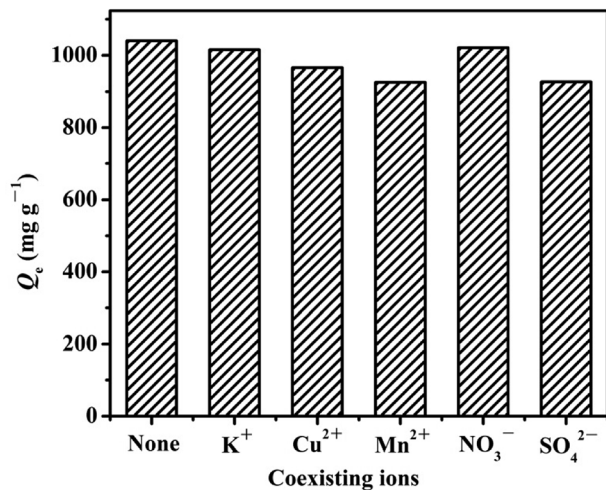
Fig. 9 Effects of coexisting ions on the adsorption of Cr(VI) by LHPP-1.

Fig. 10 Relationship between the cycle number of LHPPs and the corresponding Cr(VI) adsorption.

that **LHPP-1** exhibits selective properties for removing Cr(VI) ions.

3.2.7 Reusability of the adsorbent. Adsorption–desorption experiments were conducted for four cycles to verify the reusability of the LHPPs. The experiments were performed under the conditions of pH 1, a temperature of 308 K, an oscillating rate of 180 r, an initial Cr(VI) concentration of 200 mg L^{-1}, and a contact time of 24 h. 100 mL of 0.5 mol L^{-1} phytic acid solution was used to regenerate the adsorbent. Fig. 10 shows the relationship between the regeneration cycle number of LHPPs and the corresponding Cr(VI) removal capacity. The Cr(VI) adsorption amounts for **LHPP-1**, **LHPP-2** and **LHPP-3** were 803.62 to 867.44 mg g^{-1}, 578.87 to 638.36 mg g^{-1} and 546.37 to 604.69 mg g^{-1}, respectively. The equilibrium removal capacities of the LHPPs slightly decreased with increasing cycle number. **LHPP-1**, **LHPP-2** and **LHPP-3** exhibited excellent reusability and possessed 92.64%, 90.64% and 90.35% retention after the fourth cycle, respectively. The decreases in the adsorption amounts can be ascribed to incomplete desorption of the adsorbate from the surface of the adsorbent.[61]

3.3 Adsorption mechanism study

XPS and FTIR were used to investigate the mechanism of Cr(VI) removal from aqueous solution at pH 1 by **LHPP-1**. Fig. 11(a) displays the FTIR spectra of **LHPP-1** before and after Cr(VI) adsorption. It can be seen that the intensity of the peak of **LHPP-1** at 1590 cm^{-1} increased after Cr(VI) removal, indicating that the content of the C=N groups increased in the polymer structures. The results exhibited that some units of –NH–Ph– in **LHPP-1** were oxidized to units of –N=Ph– during the Cr(VI) removal process.[61] As shown in Fig. 11(b), before adsorption, the **LHPP-1** was composed of C 1s, N 1s, O 1s and Si 2p; after adsorption, the peak position of Cr 2p was found to be in the range of 571.2 to 594.4 eV, indicating that Cr(VI) was successfully adsorbed by **LHPP-1**. Fig. 11(c) shows the characteristic binding energy peak of Cr 2p. The binding energy peaks at 588.48 and 578.98 eV correspond to Cr 2p of Cr(VI), and the binding energy peaks at 586.78 and 577.08 eV correspond to Cr 2p of Cr(III). The
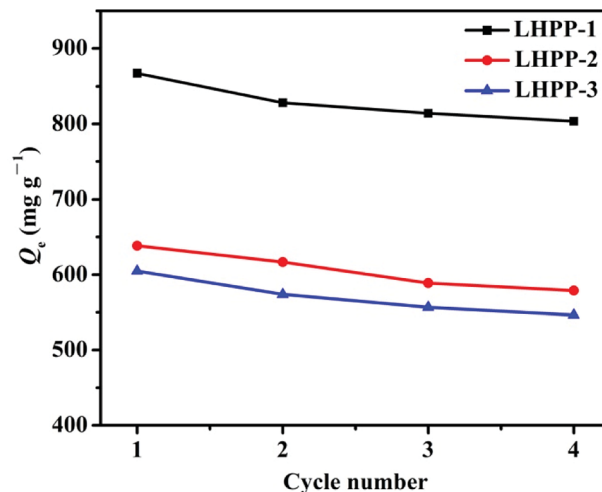
results were attributed to the partial reduction of Cr(VI) in solution to Cr(III) by **LHPP-1** during the removal process (Scheme 1).[55] Comparison of the peak areas of Cr(III) and the total Cr revealed a favorable reduction, with Cr(III) accounting for 68.9%; this indicates the good reducibility of **LHPP-1**.[41] When the pH was in the range of 1 to 6, Cr(VI) existed mainly in the forms of HCrO$_4^-$ and Cr$_2$O$_7^{2-}$ anions. The reduction of Cr(VI) to Cr(III) in acidic medium on the surface of the adsorbent is governed by the following equations.[69]

$$Cr_2O_7^{2-} + 14H^+ + 6e^- \rightarrow 2Cr^{3+} + 7H_2O \tag{9}$$

$$HCrO_4^- + 7H^+ + 3e^- \rightarrow Cr^{3+} + 4H_2O \tag{10}$$
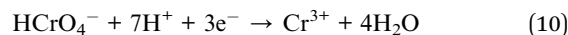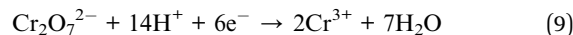
The –NH– of **LHPP-1** acted as the electron donor and –NH$^+$=/–NH$_2^+$– provided the H$^+$ in the reduction process.[38,55]
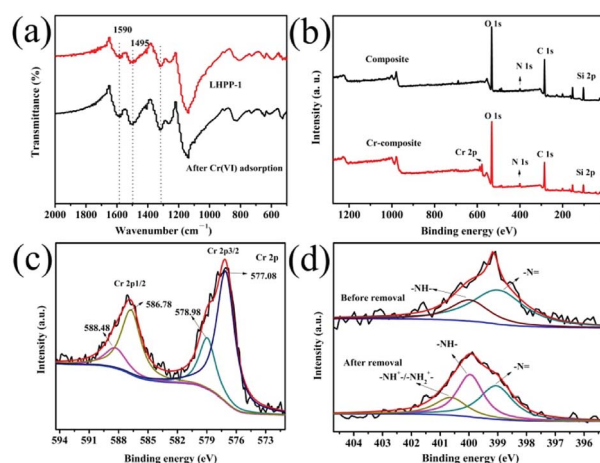

Fig. 11 (a) FTIR spectra of **LHPP-1** before and after Cr(VI) removal, (b) XPS spectra of **LHPP-1** before and after Cr(VI) removal, high resolution XPS spectra of Cr 2p (c) and N 1s (d) for **LHPP-1** before and after Cr(VI) removal.

Fig. 11(d) displays the high-resolution XPS of the N 1s peak before and after Cr(VI) adsorption in solution. Before adsorption, two binding energy peaks existed at 399.1 and 400.0 eV, corresponding to the –N= and –NH– groups, respectively. After adsorption, a new binding energy peak of –NH$^+$=/–NH$_2$$^+$– appeared at 400.7 eV.[70] The reason for the new peak of –NH$^+$=/–NH$_2$$^+$– is that some –N= and –NH– groups were readily protonated to –NH$^+$=/–NH$_2$$^+$– under the acidic conditions. This provided sufficient adsorption sites for efficient adsorption of Cr(VI).[41] Based on the analysis, the removal mechanism of the LHPPs for Cr(VI) was attributed to three aspects (Scheme 1). Firstly, Cr(VI) was adsorbed by the adsorbent *via* electrostatic attraction interactions with –NH$^+$=/–NH$_2$$^+$–; secondly, most of the Cr(VI) accepted electrons from –NH– units and were then reduced to Cr(III), while the units of –NH– were oxidized to units of –N=; third, most of the Cr(III) cations were chelated with units of –N=Ph=N– and adsorbed by **LHPP-1**.[71] In this process, the electrostatic attraction and simultaneous reduction are chiefly responsible for the highly efficient Cr(VI) removal performance in this work. This result was similar to other reports.[72]

4   Conclusions

In summary, we have demonstrated a facile method to prepare hybrid porous polyanilines for highly efficient Cr(VI) removal. During the synthesis of the hybrid porous polyanilines, commonly used leucoemeraldine and OVS were directly used as the building unit and the cross-linker, respectively. The apparent surface areas of the as-synthesized LHPPs were in the range of 147 to 388 m^2 g^{-1} and the total volumes were in the range of 0.13 to 0.44 cm^3 g^{-1}. The porosities of the LHPPs could be tuned by changing the mass ratio of OVS to leucoemeraldine. The Cr(VI) removal performance of the LHPPs was investigated by batch adsorption experiments. The results indicated that the Cr(VI) removal capacity was strongly dependent on the solution pH, the composition of the adsorbent, the initial concentration of Cr(VI), the contact time and the adsorption temperature. The adsorption process was endothermic and spontaneous and conformed to the Langmuir isotherm model as well as the pseudo-second-order kinetic model. Under the conditions of pH 1.0 and 308 K, **LHPP-1** possessed the optimum Cr(VI) removal performance. The maximum removal capacity was 990.1 mg g^{-1}, which is higher than those of other polyaniline-based adsorbents. The presence of numerous amine and imine groups as well as the porous structure of **LHPP-1** were confirmed to be responsible for its high removal capacity for Cr(VI). The effects of coexisting ion experiments revealed that **LHPP-1** displays excellent adsorption selectivity to Cr(VI) regardless of the presence of cations (K$^+$, Cu^{2+}, Mn^{2+}) and anions (NO^{3-}, SO$_4$$^{2-}$). Therefore, the present study may provide a new approach for the development of polyaniline-based adsorbents for environmental remediation.

Conflicts of interest

There are no conflicts to declare.

Notes and references

1 R. Karthik and S. Meenakshi, Synthesis, *Int. J. Biol. Macromol.*, 2015, **72**, 235.
2 M. Bhaumik, S. Agarwal, V. K. Gupta and A. Maity, *J. Colloid Interface Sci.*, 2016, **470**, 257.
3 H. Wang, X. Yuan, Y. Wu, X. Chen, L. Leng, H. Wang, H. Li and G. Zeng, *Chem. Eng. J.*, 2015, **262**, 595.
4 X. Guo, G. Fei, H. Su and L. Zhang, *J. Phys. Chem. C*, 2011, **115**, 1608.
5 A. Olad and R. Nabavi, *J. Hazard. Mater.*, 2007, **147**, 845.
6 T. Zhou, C. Li, H. Jin, Y. Lian and W. Han, *ACS Appl. Mater. Interfaces*, 2017, **9**, 6030.
7 A. G. Yavuz, E. Dincturk-Atalay, A. Uygun, F. Gode and E. Aslan, *Desalination*, 2011, **279**, 325.
8 Q. Li, L. Sun, Y. Zhang, Y. Qian and J. Zhai, *Desalination*, 2011, **266**, 188.
9 G. Sharma, M. Naushad, A. Al-Muhtaseb, A. Kumar, M. R. Khan, S. kalia, Shweta, M. Bala and A. Sharma, *Int. J. Biol. Macromol.*, 2017, **95**, 484.
10 S. Zhang, M. Zeng, W. Xu, J. Li, J. Li, J. Xu and X. Wang, *Dalton Trans.*, 2013, **42**, 7854.
11 G. Wang, Y. Hua, X. Su, S. Komarneni, S. Ma and Y. Wang, *Appl. Clay Sci.*, 2016, **124**, 111.
12 J. Yang, M. Yu and W. Chen, *J. Ind. Eng. Chem.*, 2015, **21**, 414.
13 W. Jiang, Q. Cai, W. Xu, M. Yang, Y. Cai, D. D. Dionysiou and K. E. O'Shea, *Environ. Sci. Technol.*, 2014, **48**, 8078.
14 Y. Zou, X. Wang, A. Khan, P. Wang, Y. Liu, A. Alsaedi, T. Hayat and X. Wang, *Environ. Sci. Technol.*, 2016, **50**, 7290.
15 J. Li, X. Wang, G. Zhao, C. Chen, Z. Chai, A. Alsaedi, T. Hayat and X. Wang, *Chem. Soc. Rev.*, 2018, **47**, 2322.
16 S. Yu, X. Wang, H. Pang, R. Zhang, W. Song, D. Fu, T. Hayat and X. Wang, *Chem. Eng. J.*, 2018, **333**, 343.
17 P. Gu, S. Zhang, X. Li, X. Wang, T. Wen, R. Jehan, A. Alsaedi, T. Hayat and X. Wang, *Environ. Pollut.*, 2018, **240**, 493.
18 G. Zhao, X. Huang, Z. Tang, Q. Huang, F. Niua and X. Wang, *Polym. Chem.*, 2018, **9**, 3562.
19 H. Chen, J. Dou and H. Xu, *Appl. Surf. Sci.*, 2017, **425**, 728.
20 Y. Jiang, Z. Liu, G. Zeng, Y. Liu, B. Shao, Z. Li, Y. Liu, W. Zhang and Q. He, *Environ. Sci. Pollut. Res.*, 2018, **25**, 6158.
21 V. Mazeiko, A. K. Minkstimiene, A. Ramanaviciene, Z. Balevicius and A. Ramanavicius, *Sens. Actuators, B*, 2013, **189**, 187.
22 S. H. Qiu, C. Chen, W. R. Zheng, W. Li, H. C. Zhao and L. P. Wang, *Synth. Met.*, 2017, **229**, 39.

23 M. Mohsennia, M. M. Bidgoli, F. A. Boroumand and A. M. Nia, *J. Mater. Sci. Eng. B*, 2015, **197**, 25.

24 M. A. Moussa, M. H. A. Rehim, S. A. Khairy, M. A. Soliman, A. M. Ghoneim and G. M. Turky, *Synth. Met.*, 2015, **209**, 34.

25 Q. Li, L. Sun, Y. Zhang, Y. Qian and J. Zhai, *Desalination*, 2011, **266**, 188.

26 D. Moon, M. Ezuka, T. Maruyama, K. Osakada and T. Yamamoto, *Macromol. Chem. Phys.*, 1993, **194**, 3149.

27 R. Karthik and S. Meenakshi, *Int. J. Biol. Macromol.*, 2014, **67**, 210.

28 J. J. Alcaraz-Espinoza, A. E. Chavez-Guajardo, J. C. Medina-Llamas, C. A. S. Andrade and C. P. de Melo, *ACS Appl. Mater. Interfaces*, 2015, **7**, 7231.

29 M. Bhaumik, A. Maity, V. V. Srinivasu and M. S. Onyango, *Chem. Eng. J.*, 2012, **181**, 323.

30 J. Q. Wang, K. Pan, E. P. Giannelis and B. Cao, *RSC Adv.*, 2013, **3**, 8978.

31 N. Wang, Y. Chen, J. Y. Ren, X. Y. Huang, X. Y. Chen, G. D. Li and D. Q. Liu, *J. Polym. Res.*, 2017, **24**, 42.

32 D. Xu, S. Yan, W. Weng and R. Xiao, *RSC Adv.*, 2016, **6**, 44723.

33 X. Luo, A. J. Killard, A. Morrin and M. R. Smyth, *Chem. Commun.*, 2007, **30**, 3207.

34 B. K. Kuila and M. Stamm, *J. Mater. Chem.*, 2010, **20**, 6086.

35 C. J. Weng, Y. L. Chen, Y. S. Jhuo, L. Y. Li and J. M. Yeh, *Polym. Int.*, 2013, **62**, 774.

36 H. D. Tran, J. M. D'Arcy, Y. Wang, P. J. Beltramo, V. A. Strong and R. B Kaner, *J. Mater. Chem.*, 2011, **21**, 3534.

37 W. Chen, R. B. Rakhi and H. N. Alshareef, *J. Mater. Chem. A*, 2013, **1**, 3315.

38 Q. Hu, C. Guo, D. Sun, Y. Ma, B. Qiu and Z. Guo, *ACS Sustainable Chem. Eng.*, 2017, **5**, 11788.

39 S. Zhang, M. Zeng, W. Xu, J. Li, J. Li, J. Xu and X. Wang, *Dalton Trans.*, 2013, **42**, 7854.

40 D. Z. Chen, S. P. Yi, W. B. Wu, Y. L. Zhong, J. Liao, C. Huang and W. J. Shi, *Polymer*, 2010, **51**, 3867.

41 Z. Zhang, T. Gao, S. Si, Q. Liu, Y. Wu and G. Zhou, *Chem. Eng. J.*, 2018, **343**, 207.

42 J. Huang and R. B. Kaner, *Angew. Chem.*, 2004, **116**, 5941.

43 F. Guo, Q. Liu and H. Mi, *Mater. Lett.*, 2016, **163**, 115.

44 R. Ullah, H. Ullah, A. A. Shah, B. Bilal and K. Ali, *J. Mol. Struct.*, 2017, **1127**, 734.

45 D. Moon, M. Ezuka, T. Maruyama, K. Osakada and T. Yamamoto, *Macromol. Chem. Phys.*, 1993, **194**, 3149.

46 J. Germain, J. M. J. Frechet and F. Svec, *J. Mater. Chem.*, 2007, **47**, 4989.

47 V. Sharma, A. Sahoo, Y. Sharma and P. Mohanty, *RSC Adv.*, 2015, **5**, 45749.

48 T. Li, Z. Qin, B. Liang, F. Tian, J. Zhao, N. Liu and M. Zhu, *Electrochim. Acta*, 2015, **177**, 343.

49 Y. Wu, D. Wang, L. Li, W. Yang, S. Feng and H. Liu, *J. Mater. Chem. A*, 2014, **2**, 2160.

50 M. E. Abdelhamid, G. A. Snook and A. P. O'Mullane, *Langmuir*, 2016, **32**, 8834.

51 M. Saad, H. Tahir, J. Khan, U. Hameed and A. Saud, *Ultrason. Sonochem.*, 2017, **34**, 600.

52 Y. Yan, Q. Cheng, Z. Zhu, V. Pavlinek, P. Saha and C. Li, *J. Power Sources*, 2013, **240**, 544.

53 X. Wang, J. Deng, X. Duan, D. Liu, J. Guo and P. Liu, *J. Mater. Chem. A*, 2014, **2**, 12323.

54 T. T. Luo, X. K. Tian, C. Yang, W. J. Luo, Y. L. Nie and Y. X. Wang, *J. Agric. Food Chem.*, 2017, **65**, 7153.

55 K. Gong, Q. Hu, Y. Xiao, X. Cheng, H. Liu, N. Wang, B. Qiu and Z. Guo, *J. Mater. Chem. A*, 2018, **6**, 11119.

56 Q. Liu, Q. Z. Liu, W. Ma, W. L. Liu, X. X. Cai and J. S. Yao, *Colloids Surf., A*, 2016, **511**, 8.

57 Q. Liu, Q. Liu, Z. Wu, Y. Wu, T. Gao and J. Yao, *ACS Sustainable Chem. Eng.*, 2017, **5**, 1871.

58 C. Lei, X. Zhu, B. Zhu, C. Jiang, Y. Le and J. Yu, *J. Hazard. Mater.*, 2017, **321**, 801.

59 M. O. Ansari, R. Kumar, S. A. Ansari, S. P. Ansari, M. A. Barakat, A. Alshahrie and M. H. Cho, *J. Colloid Interface Sci.*, 2017, **496**, 407.

60 M. Bhaumik, V. K. Gupta and A. Maity, *J. Environ. Chem. Eng.*, 2018, **6**, 2514.

61 T. Wen, Q. Fan, X. Tan, Y. Chen, C. Chen, A. Xu and X. Wang, *Polym. Chem.*, 2016, **7**, 785.

62 J. Wang, X. Wang, G. Zhao, G. Song, D. Chen, H. Chen, J. Xie, T. Hayat, A. Alsaedi and X. Wang, *Chem. Eng. J.*, 2018, **334**, 569.

63 W. Cheng, C. Ding, X. Wang, Z. Wu, Y. Sun, S. Yu, T. Hayat and X. Wang, *Chem. Eng. J.*, 2016, **293**, 311.

64 J. Wang, P. Wang, H. Wang, J. Dong, W. Chen, X. Wang, S. Wang, T. Hayat, A. Alsaedi and X. Wang, *ACS Sustainable Chem. Eng.*, 2017, **5**, 7165.

65 T. Wen, J. Wang, S. Yu, Z. Chen, T. Hayat and X. Wang, *ACS Sustainable Chem. Eng.*, 2017, **5**, 4371.

66 Z. Chen, D. Wei, Q. Li, X. Wang, S. Yu, L. Liu, B. Liu, S. Xie, J. Wang, D. Chen, T. Hayat and X. Wang, *J. Cleaner Prod.*, 2018, **181**, 745.

67 J. Wang, Y. Liang, Q. Jin, J. Hou, B. Liu, X. Li, W. Chen, T. Hayat, A. Alsaedi and X. Wang, *ACS Sustainable Chem. Eng.*, 2017, **5**, 5550.

68 M. Bhaumik, H. J. Choi, M. P. Seopela, R. I. McCrindle and A. Maity, *Ind. Eng. Chem. Res.*, 2014, **53**, 1214.

69 J. Li, T. Peng, Y. Zhang, C. Zhou and A. Zhu, *Sep. Purif. Technol.*, 2018, **201**, 120.

70 T. Zhou, C. Li, H. Jin, Y. Lian and W. Han, *ACS Appl. Mater. Interfaces*, 2017, **9**, 6030.

71 G. Yang, L. Tang, Y. Cai, G. Zeng, P. Guo, G. Chen, Y. Zhou, J. Tang, J. Chen and W. Xiong, *RSC Adv.*, 2014, **4**, 58362.

72 C. Zhu, F. Liu, L. Song, H. Jiang and A. Li, *Environ. Sci.: Nano*, 2018, **5**, 487.